ATMOSPHERIC SCIENCE LETTERS
Atmos. Sci. Let. (2010)
Published online in Wiley Online Library
(wileyonlinelibrary.com) **DOI:** 10.1002/asl.296

RMetS
Royal Meteorological Society

Mapping Rift Valley fever and malaria risk over West Africa using climatic indicators

C. Caminade,[1]* J. A. Ndione,[2] C. M. F. Kebe,[3] A. E. Jones,[1] S. Danuor,[4] S. Tay,[4] Y. M. Tourre,[5,6] J-P. Lacaux,[7] C. Vignolles,[8] J. B. Duchemin,[9] I. Jeanne[9] and A. P. Morse[1]

[1]*School of Environmental Sciences, University of Liverpool, Liverpool L69 7ZT, UK*
[2]*CSE, Centre de Suivi Ecologique, Dakar, Senegal*
[3]*UCAD, Université Cheikh Anta Diop, Dakar, Senegal*
[4]*KNUST, Kwame Nkrumah University of Science and Technology, Kumasi, Ghana*
[5]*Meteo-France, Department of Climatogy, Analyses et Veille Hydro-Climatique (AVH), Toulouse, France*
[6]*Lamont-Doherty Earth Observatory (LDEO) of Columbia University, Palisades, USA*
[7]*OMP – Laboratoire d'Aérologie, Toulouse*
[8]*CNES, Centre National d'Etude Spatiale, Toulouse, France*
[9]*CERMES, Centre de Recherche Médicale et Sanitaire, Niamey, Niger*

**Correspondence to:*
C. Caminade, School of Environmental Science, Roxby Building, University of Liverpool, Liverpool L69 7ZT, UK.
E-mail:
Cyril.Caminade@liverpool.ac.uk

Received: 9 February 2010
Revised: 12 July 2010
Accepted: 18 August 2010

Abstract

The aim of this study is to highlight the recent progress in mapping vector-borne diseases in West Africa using modelling and field experiments. Based on climatic indicators, methods have been developed to map Rift Valley fever (RVF) and malaria risk. Modelling results corroborate that northern Senegal and southern Mauritania appear to be critical areas for RVF outbreaks and that the malaria epidemic fringe is located at the northern edge of the Sahel. Future projections highlight that the malaria risk decreases over northern Sahel. This is related to a southward shift of the potential epidemic belt in autumn. Copyright © 2010 Royal Meteorological Society

Keywords: vector-borne diseases; malaria; Rift Valley fever; disease modelling; climate change; West Africa

1. Introduction

Climate variability is an important component in determining the incidence of a number of diseases with significant human/animal health and socioeconomic impacts. This is particularly the case for low-income countries. The influence of climate variability on health in Africa is widely recognised (Thomson *et al*., 2006) and the economic development in Africa is severely affected by human and animal diseases (Sachs and Malaney, 2002). The most important diseases affecting health are vector borne, such as malaria, Rift Valley fever (RVF) and including those that are tick borne, with over 3 billion of the world population at risk. Malaria alone is responsible for at least 1 million deaths annually, with 80% of malaria deaths occurring in sub-Saharan Africa (WHO, 2005). Some 12 million of these cases and 155 000 to 310 000 malaria deaths per year are in epidemic areas (Worrall *et al*., 2004) for which climate variability is the most important feature. The climate has a large impact on the incidence of vector-borne diseases; directly via the development rates and survival of both the pathogen and the vector, and indirectly through changes in the vegetation and the land-surface characteristics. The research teams involved in AMMA mainly focused on RVF and malaria in West Africa.

RVF is an acute, fever-causing viral disease that affects domestic animals and humans. The RVF virus belongs to the genus *Phlebovirus* in the family *Bunyaviridae*. This is transmitted to vertebrate hosts by infected floodwater mosquitoes, namely species of *Aedes* and *Culex*. Generally, *Aedes* vector abundance peaks in phase with the rainy season (August), whereas the *Culex* population emerges 2 months later (October). The RVF virus affects livestock (cattle, goats, sheep and camels) and causes high mortality and abortions in pregnant females. Humans can be infected by direct contact or inhalation of viraemic animal blood during slaughtering. The human symptoms are characterised by the onset of high fever, encephalitis, haemorrhagic ocular disease and this can sometimes lead to death (Meegan *et al*., 1988).

Malaria is caused by a parasite (protozoan *Plasmodium*) that is carried by the female mosquito from the *Anopheles* spp. The first symptoms consist of fever, pain, chills and aches, and sometimes nausea and diarrhoea that can lead to more serious health issues. Infection with the most severe form of the parasite, *Plasmodium falciparum*, if not promptly treated, may lead to kidney failure, seizures, mental confusion, coma and death. Epidemics of the disease can be triggered by factors affecting human, vector or parasite populations including abnormal meteorological conditions,

changes in anti-malarial programs, population movement and environmental changes (Nájera *et al.*, 1998). The mosquitoes' breeding sites and the lifecycle of the malaria parasite are both strongly connected to climate, especially rainfall, humidity and temperature.

The key findings about RVF and malaria diseases that have been raised in AMMA are highlighted in the following sections. This research is carried out using both field and modelling experiments. The observation and modelled datasets and the methodology are described in Section 2, while results are shown in Section 3. Discussion and perspectives follow in Section 4.

2. Method

Mosquito and malaria parasite samples were collected every 2 months in two villages (Banizoumbou and Zindarou, Niger). Standard sampling procedures were followed after classical guidelines (WHO). Mosquitoes were sampled by landing and spray-catches and CDC light-traps, parasites were collected from blood finger pricks of asymptomatic inhabitants on thick and thin malaria slides, Giemsa coloured and microscopically. This cross-sectional survey began in 2003 with WHO funds, was completed in 2005 by the AMMA project and received the acceptance of the National Ethics Committee of Niger.

In order to model and map both diseases, different climate datasets are used. Daily rainfall is estimated using mixed satellite and rain gauge observations from the Global Precipitation Climatology Project (GPCP) dataset (Huffman *et al.*, 2001). Rainfall and temperature from NCEP (Kalnay *et al.*, 1996) and ERAINTERIM (Uppala *et al.*, 2008) reanalysis are also used to drive the analysis. Regional climate model (RCM) simulations carried out within the ENSEMBLES project framework are employed (Van Der Linden *et al.*, 2009). Eight RCMs are employed: KNMI-RACMO2.2b, SMHIRCA, DMI-HIRHAM, METNO-HIRHAM, METO-HC_HadRM3.0, GKSS-CCLM4.8, MPI-REMO and ICTP-REGCM3. Two types of simulations performed for the African domain (50 km^2 resolution) are examined. The first ensemble is driven at the boundaries by the ERAINTERIM reanalysis. The second ensemble is driven at the boundaries by future projections from two different General Circulation Models (GCMs) which are forced by the SRESA1B emission scenario (according to this plan: http://ensemblesrt3.dmi.dk/091 211_AMMA-Matrix.pdf).

The Liverpool Malaria Model (LMM) is a dynamic model driven by daily rainfall and temperature to simulate malaria incidence in the human population (Hoshen and Morse, 2004; Morse *et al.*, 2005). The mosquito population is simulated using larval and adult stages, with the number of eggs deposited into breeding sites and the larval mortality rate depending on the previous 10 days' rainfall. The adult mosquito

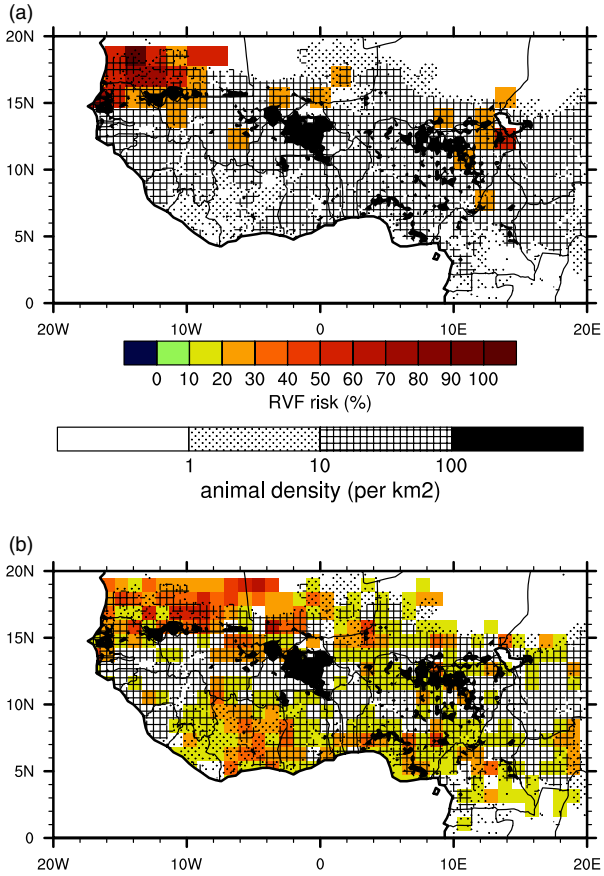

Figure 1. Rift Valley fever risk (%) based on rainfall from (a) the ERAINTERIM reanalysis (1990–2007) and (b) the GPCP (1996–2007). The number of RVF risk events is defined by a dry spell (10 consecutive days with total rainfall below 1 mm) followed by a convective event (high precipitation defined by 1 or 2 days following the dry spell above the 90th percentile) occurring during the late rainy season (SON). The total number of RVF risk events is then rescaled to range between 0 and 100% to define the risk. The dotted, crossed and filled black areas depict animal host densities (cattle + buffalo + sheep + goats) above 1, 10 and 100 per km^2 (FAO, 2005).

mortality rate and the egg-laying/biting (gonotrophic) cycle depend on temperature. Then, the process of parasite transmission between humans and mosquitoes is modelled, with temperature dependencies in the rate of development of the parasite within the mosquito (sporogonic cycle) and the mosquito biting rate. Both cycles evolve as a function of the number of 'degree days' above a specific temperature threshold. The gonotrophic (sporogonic) cycle takes approximately 37 (111) degree days with a threshold of 9 °C (18 °C). The model does not have immunity; therefore, the data from non-epidemic regions is only for non-immune members of the population.

A methodology to track the climatic events that can favour RVF risk over West Africa has been developed. These events are defined as a rainfall peak (the 90th percentile of rainfall distribution, about 10 mm) which follows a dry spell (10 consecutive days with an average below 1 mm) and this is done for the late rainy season [September–October–November (SON)]. The total number of these events is then rescaled between

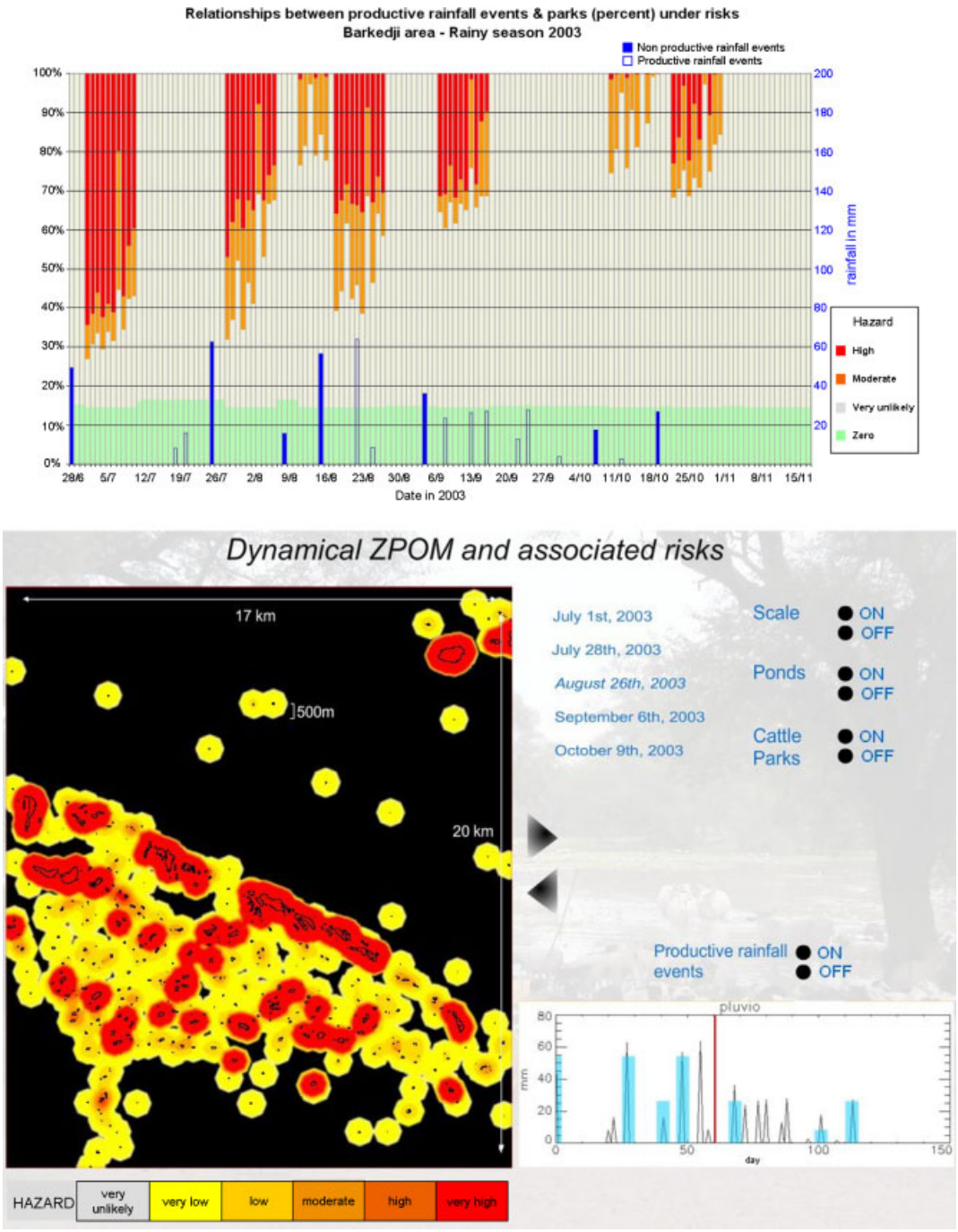

Figure 2. (Top) Relationships between productive rainfall events and percentage of parks within the ZPOM and with animals under risks. (Bottom) Dynamical ZPOMs and associated risks. Ranked risks from the 2003 summer monsoon are displayed from unlikely (yellow) to high (red). From TRMM data rainfall events, amounts (in mm) producing RVF vectors are given (vertical blue lines). From Vignolles C, Lacaux J-P, Tourre YM, Bigeard G, Ndione JA, Lafaye M. 2009. Rift Valley fever in a zone potentially ocupied by *Aedes vexans* in Senegal : dynamics and risk mapping. *Geospatial Health* **3** (2): 211–220.

0 and 100% to define the risk. Animal densities (including cattle, buffalo, sheep and goats) from the FAO archive (FAO, 2005) are then overlaid upon the climatic risk to highlight hot-spot regions.

3. Results

3.1. Rift Valley fever

The work carried out in AMMA highlighted that intra-seasonal rainfall variability is shown to be a key factor in generating high RVF risk over Senegal (Ndione *et al*., 2003, 2008). In these studies, observed RVF outbreaks are related to a long dry spell which is followed by an intense rainfall event during the late rainy season (SON). The *Culex* mosquito eggs are then rehydrated in the ponds; this leads to massive hatching in SON and unfortunately coincides with the proximity of available hosts as the farmers move the cattle near the ponds to water them during this period of the year. These climatic features have been observed for different pond regions over Senegal during the RVF

outbreaks in 1993, 1994, 1999 and 2002. Based on these results for Senegal, we extrapolated the RVF risk over West Africa (Section 2). Figure 1(a) and (b) depict the derived mean RVF risk based on ERAINTERIM rainfall for the period 1990–2007 and GPCP rainfall for the period 1996–2007, respectively. High RVF risk is highlighted over northern Senegal, southern Mauritania and central/northern Mali. If GPCP is used as the reference rainfall dataset (Figure 1(b)), the RVF risk spreads over a larger area including the Côte d'Ivoire and Nigeria. Over northern Senegal, high RVF risk is reproduced by the ERAINTERIM reanalysis during the observed RVF outbreaks in 1993, 1994 and 2002; and GPCP highlights the highest RVF risk for 1999 and 2002 (not shown). The differences between ERAINTERIM and GPCP arise from different sources. The spatial resolution and the time period availability differ for these datasets. Moreover, ERAINTERIM is based on data assimilation, whereas GPCP rainfall is a reconstruction based on satellite and rain gauge measurements. ERAINTERIM overestimates the number of rainy days near the Guinean coast for the late rainy season with respect to GPCP (not shown). Climatic factors are important, but if the livestock is not in contact with the infected mosquitoes, nothing happens. High animal densities are highlighted over northern Senegal, the southern boundary of Mauritania, central Mali and northern and coastal Nigeria (Figure 1). The superposition between the host availability and the climatic risk suggests that the northern part of Senegal and southern Mauritania are the RVF hot spots in West Africa. However, this method of defining the RVF risk based on coarse climate datasets is not relevant for regional-local scale applications.

Another methodology based on field measurements and high-spatial resolution (10 m) satellite imagery from SPOT-5 has been developed to highlight RVF hot spots at the regional scale over northern Senegal during the 2003 rainy season (Lacaux *et al.*, 2007; Tourre *et al.*, 2008; Vignolles *et al.*, 2009). This study undertaken in the Barkedji area of the Ferlo region in Senegal, during the 2003 rainy season, is based on the analysis of the interaction between the various variables associated with RVF such as the mosquito vector, available hosts and rainfall distribution. The abundance of RVF vectors is directly linked to pond dynamics and their vegetation cover and turbidity degree. The pond dynamics is associated with the spatio-temporal variability of rainfall events (Ndione *et al.*, 2003). So first, ponds considered as breeding sites were identified by remote sensing, using a high-spatial resolution SPOT-5 satellite image. A decision-tree conditional classifier based on the normalised difference pond index (NDPI) has been used to locate the temporary ponds (Lacaux *et al.*, 2007). Then, additional data on ponds and rainfall events from the Tropical Rainfall Measuring Mission were combined with *in situ* entomological (embryogenesis, aggressiveness and flying range) and limnimetric measurements, and the localization of vulnerable ruminant

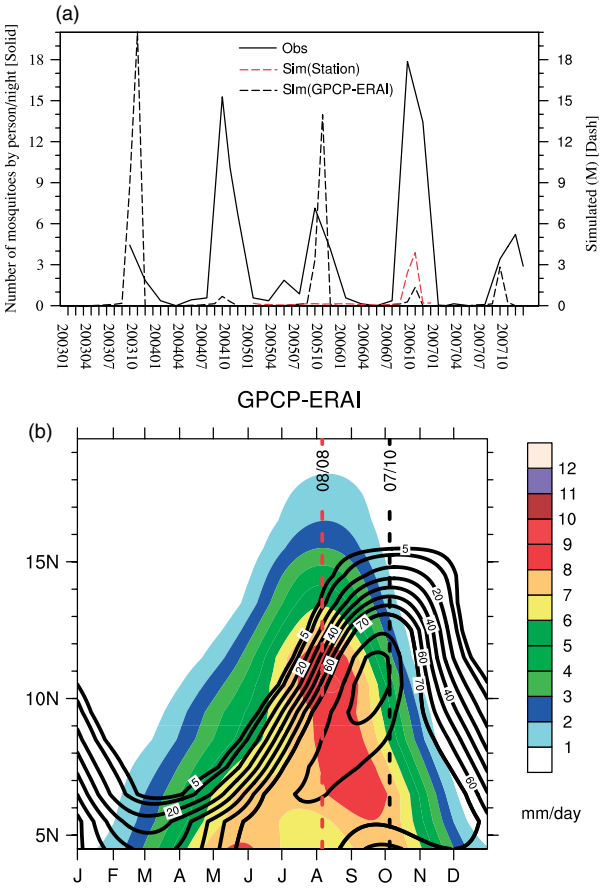

Figure 3. (a) Mean observed number of landing caught *Anopheles gambiae* s.s. mosquitoes (solid line) in Banizoumbou (13.32 °N, 2.40 °E), Niger. The dotted lines depict the number of simulated infected mosquitoes (M) as simulated by LMM using daily rainfall and temperature from station measurements (red) and daily rainfall from GPCP combined with daily temperature from ERAINTERIM (black, the closest grid point is considered). (b) Mean seasonal cycle of rainfall (shading) over West Africa (averaged between 16 °W and 16 °E) based on the GPCP data for the period 1996–2007. The mean seasonal cycle of simulated malaria incidence (cases per 100 people) is depicted by the black contours (LMM driven by GPCP rainfall and ERAINTERIM temperature over the same time window). The red (black) vertical dotted line highlights the top northward location of the rainbelt (the malaria incidence belt).

hosts (data derived from QuickBird satellite). Since '*Aedes vexans* productive rainfall events' are dependent on the timing of rainfall for their embryogenesis (6 days without rain are necessary to trigger hatching), the dynamic spatio-temporal distribution of *Aedes vexans* density was based on the total rainfall amount and pond dynamics. So mapping of detailed zones potentially occupied by mosquitoes (ZPOM) (Figure 2, bottom) was obtained on a daily basis and combined with aggressive temporal profiles. Risks zones, i.e. zones where hazards and vulnerability are combined, are expressed by the percentages of parks where animals are potentially exposed to mosquito bites (Figure 2, top). As shown in Figure 2 (top), 15% of the fenced-in ruminants were never at risk, whilst 60 to 30% of the fenced-in areas exposed the animals to moderate

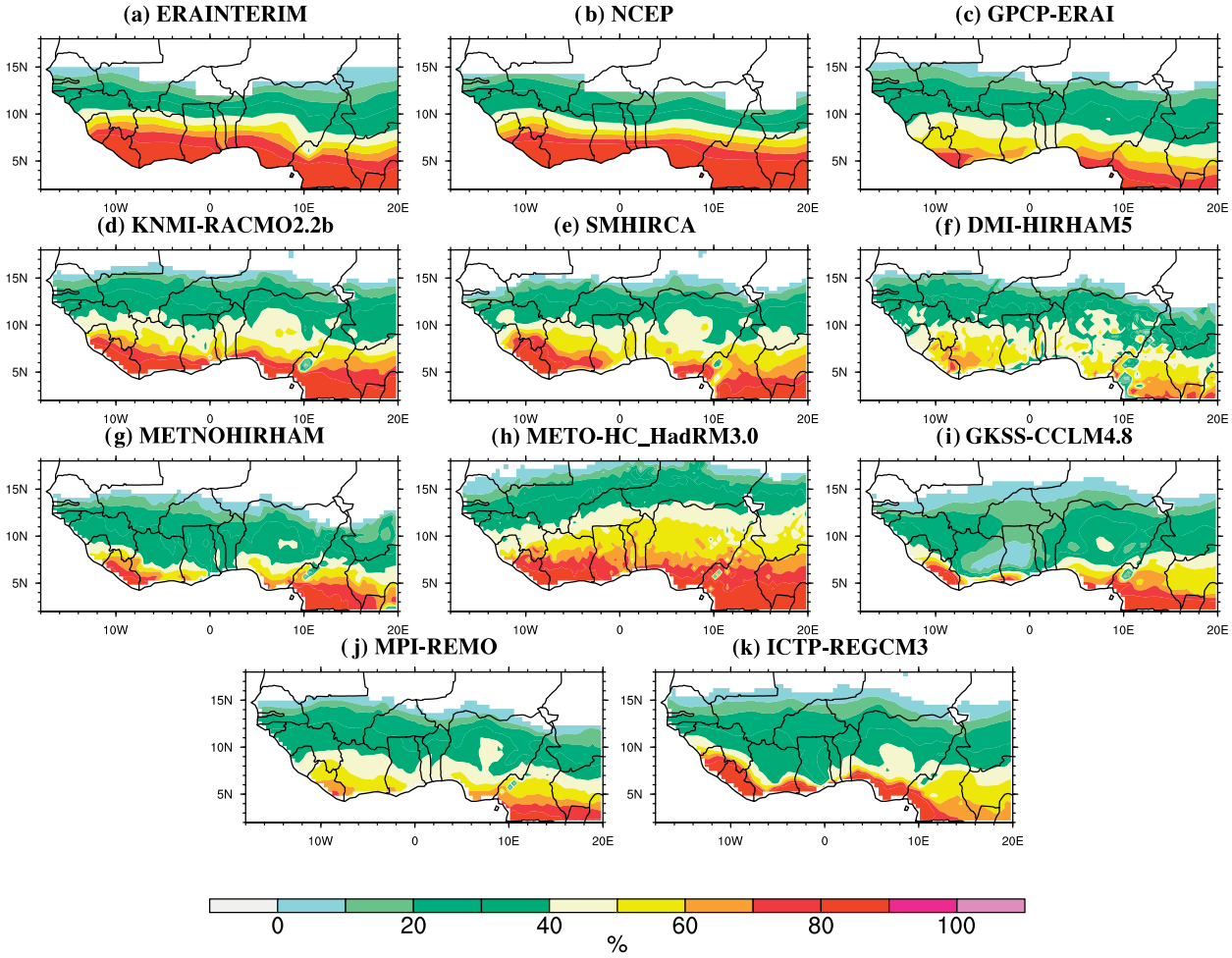

Figure 4. Mean annual malaria incidence (cases per 100 people) as simulated by LMM over West Africa for the 1990–2007 period. The LMM control simulation is driven by (a) ERAINTERIM, (b) the NCEP reanalysis and (c) rainfall from GPCP and temperature from ERAINTERIM (the period to compute the mean is 1996–2007 in this case). (d)–(k) LMM is forced by rainfall and temperature from eight RCMs that have been driven by the ERAINTERIM reanalysis at the boundaries (simulations performed within the ENSEMBLES project framework).

to high risk. This major achievement is meant to contribute to the development of a new operational early warning system (EWS) for the occurrence of RVF vectors over Senegal.

3.2. Malaria

Previous work found positive forecast skill for the prediction of epidemic malaria in Botswana (Thomson *et al*., 2006) based on multi-model seasonal forecasts, but no such assessment has been carried out for West Africa. Recent results show that the LMM was able to simulate realistic epidemic malaria prediction over West Africa, based on the ENSEMBLES multi-model seasonal forecasts (Jones and Morse, 2010). This is true for both low and high malaria categories, the multi-model being the most skilful estimate to forecast malaria incidence. This framework can be applied to operational forecasts in order to provide malaria probabilistic risk estimates at seasonal time scales.

Field experiments carried out within AMMA corroborated the relationship between malaria incidence and climate parameters (rainfall, humidity and temperature) in Kumasi (Ghana). In Banizoumbou (Niger), the total mosquito abundances showed strong seasonal patterns, peaking in August in link with the Sahel water cycle. The inter-annual variability was important and could not be directly related to the annual total rainfall. The differences between the two villages (Zindarou and Banizoumbou) underlined the spatial variability in the Sahel even at short distances (30 km). Local fine-scale models based on hydrology processes found again these between-year and between-village differences (Bomblies *et al*., 2009). The malaria parasite carriage among people showed a seasonal pattern, peaking in October, but the differences between villages was less marked. The simulated mean seasonal cycle of the abundance of infected mosquitoes for this area fits the observed dataset (Figure 3(a)). The maximum is simulated in October as for the observed parasite carriage but the inter-annual variability is not well captured (arising from biases in LMM and the climate datasets but also due to vector control measures led by the Ministry of Health of Niger). Figure 3(b) provides a larger view of rainfall and malaria dynamics

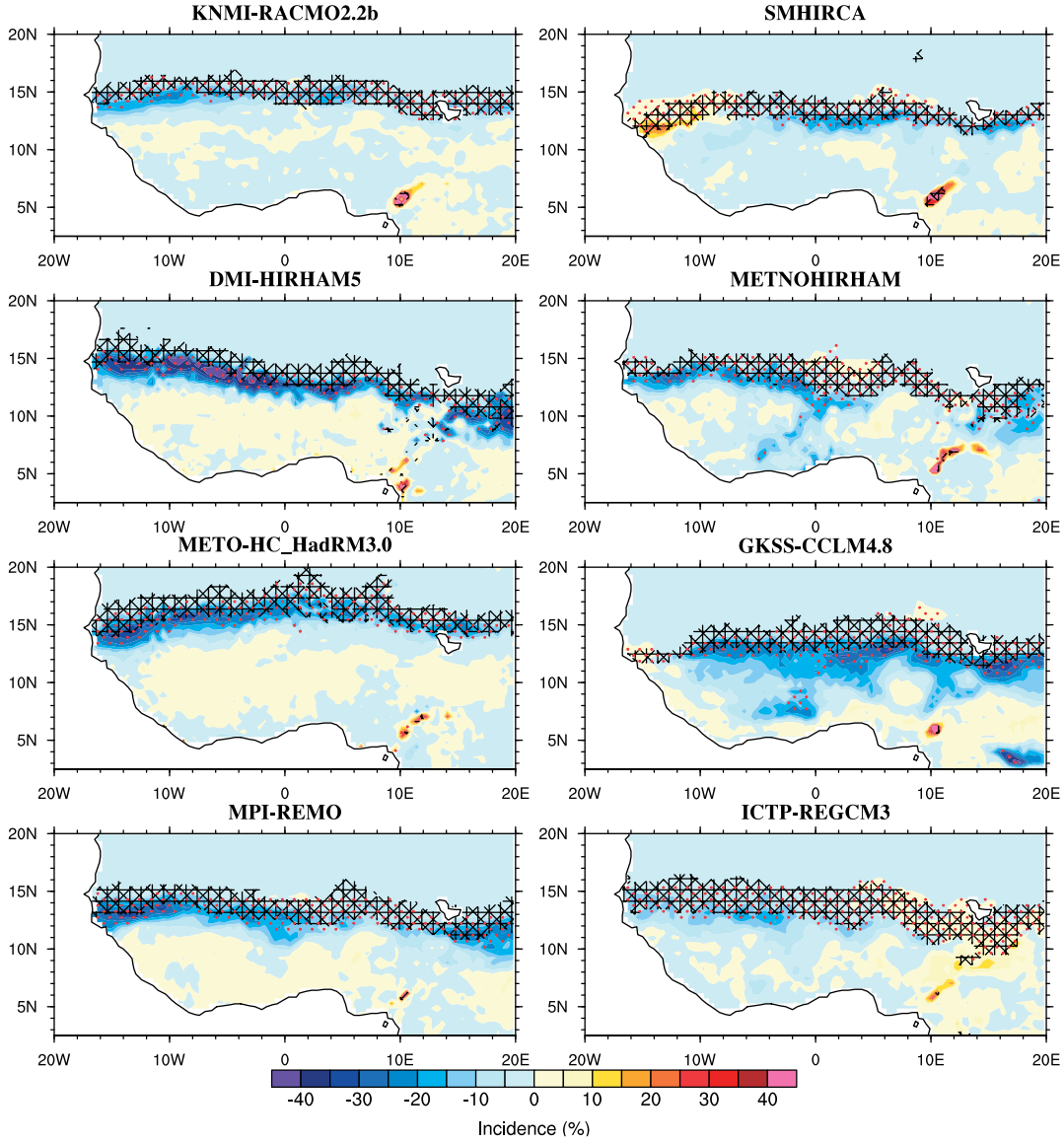

Figure 5. Mean seasonal (SON) future changes of malaria incidence (shading) as simulated by eight RCMs forced by the SRESA1B scenario (simulations performed within the ENSEMBLES project framework). The differences are computed between the time slices 2031–2050 and 1990–2010. The mean seasonal (SON) location of the 'epidemic' fringe is depicted by crosses for the recent climate (1990–2010), whereas the future pattern (2031–2050) is depicted by the red dots for each model. The epidemic belt is defined for mean incidence above the 1% threshold and when the standard deviation is above 50% of the average.

at seasonal time scales over West Africa. The onset of the West African monsoon occurs in July and the rain belt reaches its top northward location (18°N) in August over the Sahel, followed by a rapid retreat to the south in September. The malaria incidence belt reaches its top northward location (15°N) in autumn (SON). There is a phase shift between rainfall and malaria incidence seasonality. High malaria incidences are conditioned by the climatic conditions occurring 2 months before. These findings are consistent with the results raised by field observations. However, the LMM underestimates the top northward location of the malaria incidence belt. Other modelling approaches show that the northern epidemic fringe of malaria incidence spreads to 17°N (Le Sueur *et al.*, 1997).

The simulated annual mean incidence (driven by climate observations and reanalysis) highlights a clear south–north gradient pattern, with minimum incidences reaching the latitude 15°N (Figure 4(a)–(c)). High incidences show where malaria is endemic (above 70–80%, from central Africa to coastal West Africa), namely where malaria is present all year around and then mainly conditioned by human factors. Then, there is a transition zone (endemic and seasonal malaria regions) where the incidence ranges between 20 and 70%. Low annual incidence values show where malaria is epidemic and seasonal, namely strongly connected to climate variability (between 12°N and 15°N). This region is often referred to as the malaria epidemic fringe. The RCMs fairly well simulate the observation-driven incidence pattern (Figure 4(d)–(k)). However, simulated malaria incidence spreads too far north compared to the control runs because the simulated rain belt extends too far

north for these RCMs (not shown). The maximum incidence near the coasts of the Gulf of Guinea is generally underestimated by the RCM runs.

Only considering the climatic part of the malaria risk, future projections (2031–2050) highlight a decrease in mean malaria incidence over the northern epidemic fringe in autumn (Figure 5). This is consistent for the KNMI, DMI, METO-HC, MPI and GKSS model projections over the whole domain, whereas it is restricted to the central and eastern (western) part for SMHI (METNOHIRAM). The ICTP run simulates low changes. The change in the incidence variability pattern highlights a meridional dipole pattern (southward shift of the epidemic fringe). This feature is consistent across the different RCM projections (not shown). This is depicted more precisely in Figure 5, where the simulated current climate epidemic belt is compared with its future location. The potential future malaria epidemic belt is slightly shifted southward (from 1° to 2°) with respect to the current climate one. This feature is mainly related to a simulated decrease in the number of rainy days in summer over this area (not shown). Similar future changes are highlighted in another study using the LMM driven by the Remo RCM (MALARIS, 2007).

4. Discussion and perspectives

Hot-spot regions have been highlighted for RVF and malaria over West Africa, based on climatic indicators. Based on large-scale climatic indicators, we showed that northern Senegal and southern Mauritania appear to be critical areas for RVF risk in West Africa. At finer spatial scales, another method has successfully tracked the zone potentially occupied by the RVF mosquitoes over Barkedji (Senegal) in 2003. This method has demonstrated the feasibility of an operational EWS for the occurrence of RVF vectors over Senegal. Simulations performed with the LMM highlighted that the malaria epidemic fringe spreads between the latitudes 12°N and 15°N over West Africa. This fringe is strongly connected with climate variability and its northward extension is underestimated by the LMM. Future projections highlight that the malaria incidence may decrease at the northern edge of the Sahel and the potential epidemic belt may be shifted southward in autumn. As the demography is expected to increase in the future over Africa this could lead to significant health problems. However, these results must be interpreted with caution as there are still large biases related to both the disease model and to the RCM projections for the future.

Our knowledge on the links between vector-borne diseases and climate in West Africa has significantly improved during AMMA. We have to ensure that the most important results and the related uncertainties are properly transferred to society through the link of interface experts to stakeholders and policymakers. The experience and collaborations earned within AMMA will be continued in other upcoming projects in order to improve our understanding of the disease burdens in Africa under the threat of climate change.

Acknowledgements

The support by the EU projects AMMA and ENSEMBLES (funded by the European Commission's 6th Framework Programme through contract GOCE-CT 2003-505539) is gratefully acknowledged. This is LDEO contribution #7394.

References

Bomblies A, Duchemin JB, Eltahir EA. 2009. A mechanistic approach for accurate simulation of village-scale malaria transmission. *Malaria Journal* **8**: 223.

FAO. 2005. Observed and modelled livestock densities. Available from http://www.fao.org/Ag/AGAInfo/resources/en/glw/GLW_dens.html.

Hoshen MB, Morse AP. 2004. A weather-driven model of malaria transmission. *Malaria Journal* **3**: 32, DOI:10.1186/1475-2875-3-32.

Huffman GJ, Adler RF, Morrissey M, Bolvin DT, Curtis S, Joyce R, McGavock B, Susskind J. 2001. Global precipitation at one-degree daily resolution from multi-satellite observations. *Journal of Hydrometeorology* **2**(1): 36–50.

Jones AE, Morse AP. 2010. Skill of ENSEMBLES seasonal re-forecasts for epidemic malaria prediction in West Africa. AMMA Deliverable D3.4h: Assessment of potential of current R&D ensemble forecasting systems for health impact application in West Africa.

Kalnay E, Kanamitsu M, Kistler R, Collins W, Deaven D, Gandin L, Iredell M, Saha S, White G, Woollen J, Zhu Y, Leetmaa A, Reynolds R, Chelliah M, Ebisuzaki W, Higgins W, Janowiak J, Mo KC, Ropelewski C, Wang J, Jenne R, Joseph D. 1996. The NCEP/NCAR 40-year reanalysis project. *Bulletin of the American Meteorological Society* **17**(3): 437–471.

Lacaux JP, Tourre YM, Vignolles C, Ndione JA, Lafaye M. 2007. Classification of ponds from high-spatial resolution remote sensing: application to Rift Valley fever epidemics in Senegal. *Remote Sensing of Environment* **106**: 66–74.

Le Sueur D, Binka F, Lengeler C, de Savigny D, Snow RW, Teuscher T, Touréé YT. 1997. An atlas of malaria in Africa. *Africa Health* **19**: 23–24.

MALARIS. 2007. The impact of climate change on malaria risk in Africa. Available from http://www.impetus.uni-koeln.de/malaris/scenario_lmm_en.html.

Meegan JM, Bailey CL. 1988. Rift Valley fever. In *Arbovirus Epidemiology and Ecology*, Vol. IV, Monath TP (ed). CRC: Boca Raton, FL; 51–76.

Morse AP, Doblas-Reyes FJ, Hoshen MB, Hagedorn R, Palmer TN. 2005. A forecast quality assessment of an end-to-end probabilistic multi-model seasonal forecast system using a malaria model. *Tellus* **57A**: 464–475.

Nájera JA, Kouznetsov RL, Delacollette C. 1998. Malaria epidemics: detection and control, forecasting and prevention. WHO/MAL/98.1084. World Health Organization: Geneva, Switzerland. Available from http://www.who.int/malaria/docs/najera_epidemics/naj_toc.htm.

Ndione J-A, Besancenot J-P, Lacaux J-P, Sabatier P. 2003. Environnement et épidémiologie de la fièvre de la vallée du Rift (FVR) dans le bassin inférieur du fleuve Sénégal. *Environnement, Risques et Santé* **2**(3): 176–182.

Ndione JA, Diop M, Lacaux JP, Gaye AT. 2008. Variabilité intra-saisonnière de la Pluviométrie et émergence de la fièvre de la vallée du rift (FVR) dans la vallée du fleuve Sénégal : nouvelles considérations. *Climatologie* **5**: 83–97.

Sachs J, Malaney P. 2002. The economic and social burden of malaria. *Nature* **415**: 680–685.

Thomson MC, Doblas-Reyes FJ, Mason SJ, Hagedorn R, Connor SJ, Phindela T, Morse AP, Palmer TN. 2006. Malaria early warnings

based on seasonal climate forecasts from multi-model ensembles. *Nature* **439**: 576–579.

Tourre YM, Lacaux J-P, Vignolles C, Ndione JA, Lafaye M. 2008. Mapping of zones potentially occupied by mosquitoes (ZPOMs) *Aedes vexans* and *Culex poicipiles*, the main vectors of Rift Valley fever in Senegal. *Geospatial Health* **3**(1): 69–79.

Uppala S, Dee D, Kobayashi S, Berrisford P, Simmons A. 2008. *Towards a climate data assimilation system: Status update of ERA-Interim, in ECMWF Newsletter*, Vol. 115. European Centre for Medium-Range Weather Forecasts: Reading-UK; 12–18.

Van der Linden PJ, Mitchell JFB (eds). 2009. *ENSEMBLES: Climate Change and Its Impacts: Summary of Research and Results from the ENSEMBLES Project*. Met Office Hadley Centre: Exeter, UK. Details about the ENSEMBLES RCMs simulations are available from: http://ensemblesrt3.dmi.dk/.

Vignolles C, Lacaux J-P, Tourre YM, Bigeard G, Ndione JA, Lafaye M. 2009. Rift Valley fever in a zone potentially ocupied by *Aedes vexans* in Senegal : dynamics and risk mapping. *Geospatial Health* **3**(2): 211–220.

WHO. 2005. *World Malaria Report 2005*. World Health Organization: Geneva; 294. pp. Available from: http://rbm.who.int/wmr2005/html/toc.htm.

Worrall E, Rietveld A, Delacollette C. 2004. The burden of malaria epidemics and cost-effectiveness of interventions in epidemic situation in Africa. *American Journal of Tropical Medicine and Hygiene* **71**(2): 136–140.

